ARTICLE OPEN

Cardamom synergizes with cisplatin against human osteosarcoma cells by mTOR-mediated autophagy

Sheng Li[1], Ziyun Li[2], Jiayu Wang[2], Xueqian Han[2] and Lulu Zhang[3]✉

Cisplatin (DDP), a frontline chemotherapeutic agent in osteosarcoma (OS) treatment, is frequently paired with other compounds to enhance its therapeutic potency. Cardamom (CAR), a natural flavonoid, exhibits significant inhibitory effects on human OS cells while minimizing toxic side effects. In this study, we combined CAR and DDP to treat OS, revealing that the DDP/CAR combination synergistically inhibits the growth of human OS cells in vitro and in vivo. Network pharmacological analysis indicated that mammalian target of rapamycin (mTOR) may be an important cross-target for DDP/CAR combination. Notably, this combined treatment significantly reduced mTOR phosphorylation and elevated autophagy levels within OS cells. At the mechanistic level, the DDP/CAR regimen enhanced apoptosis and compromised the viability of OS cells by triggering autophagy. This impact was attenuated by the use of the mTOR activator MHY and the autophagy inhibitor hydroxychloroquine (HCQ). Furthermore, in DDP-resistant cell lines, CAR was able to mitigate DDP resistance by bolstering autophagy levels. In general, our results suggest that CAR bolstering autophagy levels DDP against OS cells through the induction of mTOR-mediated autophagy.

Cancer Gene Therapy (2025) 32:538–549; https://doi.org/10.1038/s41417-025-00894-9

Graphical Abstract

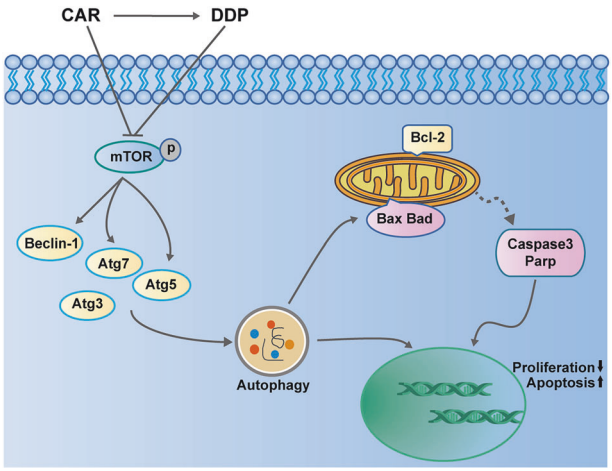

INTRODUCTION

Osteosarcoma (OS) is a most prevalent bone tumor among adolescents [1–4]. OS has the ability to rapidly proliferate and invade, and patients with OS tend to have high recurrence rate and a relatively low long-term survival rate [5]. The standard therapies for OS, including surgery and chemotherapy, have improved the prognosis of OS patients to some extent, particularly those with local diseases [4]. The most commonly utilized chemotherapy drug in OS treatment is cisplatin (DDP). Frustratingly, the outcomes of DDP monotherapy are usually unsatisfactory, especially in patients with distant metastasis or drug resistance. Moreover, patients receiving DDP treatment often experience severe toxic side effects inevitably. To address these challenges, DDP-based combination regimens such as AP (doxorubicin and DDP) and MAP (high-dose methotrexate, doxorubicin and DDP) have emerged as the primary

[1]Department of Respiratory Medicine, Shapingba Hospital affiliated to Chongqing University, Chongqing, China. [2]Key Laboratory of Clinical Laboratory Diagnostics Designated By Ministry of Education, College of Laboratory Medicine, Chongqing Medical University, Chongqing, China. [3]Department of Clinical Laboratory, Medical Sciences Research Center, University-Town Hospital of Chongqing Medical University, Chongqing, China. ✉email: 800475@hospital.cqmu.edu.cn

Received: 25 October 2024 Revised: 21 February 2025 Accepted: 14 March 2025
Published online: 26 March 2025

chemotherapy strategies employed in the treatment of OS. Besides, numerous clinical trials have evaluated the efficacy of diverse combinations of chemotherapy drugs [6–9].

Natural products (NPs) represent an abundant source of potential anti-tumor agents, with numerous clinical chemotherapy drugs for tumors having been derived from NPs or their modified structural analogs [10]. Some NPs can serve as standalone treatments to eliminate tumor cells or be combined with established chemotherapy drugs like cisplatin (DDP) to achieve a synergistic anti-neoplastic effect. For instance, the combination of bee venom and DDP can produce synergistic antitumor effects in ovarian cancer cells [11]. A previous study by our team reported that echinatin (Ecn)/DPP co-treatment produces the synergistic inhibitory effect on OS cells [12]. Cardamom (CAR) is a natural flavonoid with significant anti-tumor effects [13–15]. Our previous research has shown that CAR has the potential to suppress OS cell growth with minimal toxic side effects [16]. The objective of this study was to confirm whether CAR can act in synergy with DDP to inhibit OS cells, and to elucidate the underlying mechanisms. Our findings indicate that CAR indeed synergizes with DDP to suppress human OS cells both in vitro and in vivo, while also reducing DDP resistance. Mechanistically, the CAR/DDP combination significantly produced autophagy in OS cells by downregulating mTOR phosphorylation levels. Notably, mTOR activator MHY and autophagy inhibitor hydroxychloroquine (HCQ) not only inhibited CAR/DDP-induced autophagy level, but also decreased the apoptosis, and restored the viability of OS cells. Totally, our results indicate that CAR may inactivate mTOR, and then promote mTOR-mediated autophagy to cooperae with DDP against human OS cells.

MATERIALS AND METHODS

Reagents and cell lines

MG63, 143B and HOS OS cells were purchased from iCell Bioscience Inc (Shanghai, China). Osteosarcoma cisplatin-resistant cell lines (HOS/DDP) was purchased from MeisenCTCC (Zhejiang, China). Cells were cultured in complete DMEM (500 mL of DMEM + 50 mL fetal bovine serum) (FBS, ExCell Bio, Shanghai, China) in CO_2 incubator at 37 °C. All cell lines have been routinely tested for mycoplasma contamination.

Crystal violet assay

143B and MG63 cells were seeded in 24 well plates. Upon reaching 50% density, cells were treated with CAR (Chengdu HerpurifyCo, Ltd, China) and DDP (CuiyirunCo.,Ltd, China) for 24 h. Thereafter, the supernatant was discarded and the cell viability was evaluated by staining with crystal violet working solution (Amresco, America).

MTT assay

OS cells were exposed to treatment with CAR and DDP for 24 h. Subsequently, the solution of 5 mg/mL MTT (Solarbio, Beijing, China) was added and incubated at 37 °C for 4 h. Following incubation, the MTT solution was aspirated and replaced with 150 µL of DMSO (BioFROXX, Germany) in each well to ensure complete dissolution of the MTT formazan. Cell viability was assessed by measuring absorbance at 492 nm.

ZIP model analysis

The Zero Interaction Potency (ZIP) model is a method for capturing drug interaction relationships. It compares changes in the potency of dose-response curves (effects at specific dose levels) between individual drugs and their combinations [17]. The ZIP model was employed to assess the combined effect of CAR and DDP and to identify the most synergistic region.

EdU assay

OS cells were seeded in well plates, and when the cell density reaches 50%, CAR and DDP treatments were added. After 24 h, the EdU test was performed according to protocol ((Beyotime, China)).

Network pharmacology construction

The 3D structure of CAR and DDP was obtained from the PubChem database (https://pubchem.ncbi.nlm.nih.gov/) for subsequent backup [18]. The targets for CAR and DDP in Homo sapiens came from three databases, namely the Swiss Target Prediction (http://www.swisstargetprediction.ch) [19], the PharmMapper database (http://www.lilabecust.cn/pharmmapper/) [20] and the CTD database (https://ctdbase.org/) [21]. UniProt (https://www.uniprot.org/) Retrieve/ID mapping was used to obtain the official symbol format of the target gene [22]. Osteosarcoma-targeting genes were collected from GeneCards (https://www.genecards.org/) [23]. The intersection of the three targets (Osteosarcoma, CAR and DPP) were obtained through the Venny 2.1.0 platform for the creation of drug-disease co-targets. Protein interaction networks were created using the STRING online database (https://string-db.org/) [24] and visualized with Cytoscape software (3.8.2). The Cytohubba plugin is used to evaluate the combined network and filter out the core targets.

Flow cytometry apoptosis analysis

Apoptosis of cells was assessed with flow cytometer using the V-FITC/PI double-staining kit (Beyotime, China). Briefly, OS cells were seeded at a density of 2.5×10^5 cells/well in 6-well cell culture plates and incubated overnight for 24 h. Cells were treated with CAR and DDP for another 24 h. Following treatment with CAR and DDP for additional 24 h, cells were washed with cold PBS, trypsinized, and centrifuged at $1000 \times g$ for 3 min to harvest. After washing the cells three times with PBS, they were suspended in 500 µL of PBS, stained with the Annexin V-FITC/PI double-labeled staining kit following the manufacturer's instructions, and analyzed for cell apoptosis using flow cytometer (CytoFLEX, Beckman Coulter, USA).

Hoechst33258 staining

MG63 and 143B OS cells were seeded in 24 well plates. Upon reaching density of 50%, the cells were exposed to CAR and DDP for 24 h. Cells were washed twice with cold PBS after removing the cell culture supernatant, then fixed with 4% paraformaldehyde and stained with 10 ng/mL Hoechst33258 (Solarbio, Beijing, China) for 10 min. Three random fields were selected to capture images of the cells undergoing apoptosis using light microscopy.

Transmission electron microscopy (TEM)

MG63 and 143B OS cells were seeded in 10 cm cell culture dishes, and treated with CAR and DDP for 24 h. Cells were then trypsinized and subsequently centrifuged for precipitation. After removal of cell culture supernatant, cells were suspended and kept in 4% glutaraldehyde at 4 °C for 24 h. Then, cells were fixed with 1% osmium acid, followed by dehydration in acetone, embedding in Epon resin (EMS, Fort Washington, PA, USA), and staining with lead citrate. The ultrastructural morphology of cells was observed by transmission electron microscopy (TEM), and the representative images were collected.

Western blot

OS cells were seeded into 10 cm cell culture dishes. Upon reaching a density of 80%, the cells were exposed to CAR and DDP for 24 h. Subsequently, the cultured cells underwent cold PBS wash and were then lysed using RIPA lysis buffer with 1% protease/phosphatase inhibitors (Roche, Basel, Switzerland) for 30 min on ice. Cell lysates were centrifuged at 13,000 × *g* for 15 min, and the supernatant was collected. The concentration of protein was determined with the BCA kit (Beyotime, P0012S) following the guidelines provided by the manufacturer. Equal amounts of protein samples were separated by SDS-PAGE and were subsequently transferred to PVDF membrane. Following blocking using 5% Albumin Bovine V (Solarbio, Beijing, China), the membranes were then exposed to specific primary antibodies (Table 1) and incubated overnight at 4 °C. The membranes were washed with 1 × TBST, and then incubated with horseradish peroxidase (HRP)-conjugated secondary antibody. The target proteins were visualized by ECL kit, and photographed by gel imaging system.

OS tumor xenograft model

Female BALB/c nude mice aged 28 days and weighing 20 ± 2 g were acquired from Beijing Huafukang Biotechnology Co., Ltd. The mice were raised in 12-h light-dark cycle under specific pathogen-free (SPF) conditions at the animal center of Chongqing Medical University. Female

Table 1. List of antibodies.

Name	Vendor	Catalog number	Name	Vendor	Catalog number
p-mTOR	Affinity	AF3308	Atg5	CST	2630S
mTOR	Affinity	AF6308	Atg7	CST	2631S
β-actin	CST	4967	Bad	CST	9239
P62	CST	5114S	Bax	CST	2772
LC3	CST	12741S	Bcl-2	CST	15071
Atg3	CST	3415S	Beclin-1	CST	3495S
Parp	CST	9542	Caspase3	CST	9662
Cleaved- Parp	CST	5625	Cleaved-Caspase3	CST	9661

nude mice were injected with 143B cells at a concentration of 2×10^6 in 70 μL of PBS in the femur. After four days, the mice that had been injected were divided into four groups ($N = 3$) in random manner. These groups included the Control group, CAR group (15 mg/kg), the DDP group (3.5 mg/kg) and the CD group (CAR 15 mg/kg + DDP 3.5 mg/kg treatment). Mice were orally administered with CAR and/or DDP at specified doses every other day, with subsequent recording of body weight and tumor size. At 20 days after treatment, all mice were humanely sacrificed to collect xenograft tumors.

Immunohistochemistry

The tumor specimens were treated with 4% paraformaldehyde and embedded in paraffin (5 μm thick sections). Briefly, tumor samples were deparaffinized, hydrated, and subjected to antigen repair by incubating with sodium citrate at 100 °C in sequential manner. Following the inactivation of endogenous peroxidase, the solution of normal goat serum was introduced to prevent non-specific interactions. Next, the tumor sections were exposed to an overnight incubation at 4 °C with specific primary antibody. Afterward, the sections were exposed to secondary antibody coupled with HRP (Zsbio, Beijing, China) at room temperature for 1 h. The signal of antigen antibody complex was finally detected by DAB (Zsbio, Beijing, China).

H&E staining

Paraffin blocks were created from the tumor samples obtained from each group. 5 μm thick sections were prepared from paraffin-embedded OS samples, followed by rehydration using graded series of 100%, 90%, 80% and 70% ethanol. Afterward, the sections were stained with Hematoxylin-Eosin following the typical histopathological procedure (Solarbio, Beijing, China), and then observed and captured using light microscope.

Statistical analysis

All analyzes in this study were repeated three times. All data were represented as mean ± standard and were analyzed using GraphPad Prism 8.0 (GraphPad Software, La Jolla, CA). Statistical significance was assessed through either two-tailed Student's *t*-tests or One-way analysis of variance (ANOVA). P value < 0.05 was considered indicative of statistical significance.

RESULTS

CAR/DDP combination synergistically inhibits the proliferation of OS cells

Firstly, we confirmed the synergistic antitumor activity of the combination of CAR and DDP on OS cells. MTT assays were conducted to assess cell viability, revealing that CAR showed excellent inhibitory effects on 143B and MG63 OS cells, with 50% inhibition concentration (IC50) values of 33.1 μM and 59.1 μM, respectively (Fig. 1A). For DDP, the IC50 values in 143B and MG63 cells were 11.7 μM and 30.0 μM, respectively (Fig. 1B). Subsequently, we treated OS cells with multiple concentrations of CAR and DDP, both below their IC50 values, and evaluated their combined effects using the ZIP model, which scores synergistic interactions with a threshold greater than 10, indicating strong synergy [17]. The results (Fig. 1C) demonstrated a markedly synergistic effect of the CAR/DDP combination. Based on ZIP synergy scores, we finally selected 9 μM of CAR and 7.3 μM of DDP as the subsequent experimental concentration for 143B cells, while 9 μM of CAR and 9.3 μM of DDP for MG63 cells. Confirmation was then provided through EdU assay (Fig. 1D, E) showing that the inhibitory rate of the CAR/DDP combination group was significantly greater than that of individual drug group, indicating a strong synergistic effect. Ultimately, a xenograft model was created to validate the combined anti-OS effects of CAR and DDP in vivo. Although body weight did not significantly differ among groups (Fig. 1G), the tumor size in the CAR/DDP combination group was considerably smaller than in the monotherapy groups (Fig. 1F, H). We noticed common cancerous characteristics like darkly-colored nuclei and cytoplasm, as well as a high ratio of nuclei to cytoplasm in blank group. Noticeably, CAR, DDP, and CAR/DDP combination all demonstrated the ability to inhibit these malignant phenotypes, with CAR/DDP co-administration showing the strongest inhibitory capacity (Fig. 1I). Collectively, our data indicate that combination of CAR and DDP effectively suppress the proliferation of OS cells in vitro and in vivo.

CAR/DDP combination suppresses the activation of mTOR in OS cells

Subsequently, we embarked on a preliminary investigation to elucidate the molecular mechanisms underlying the synergistic effect of CAR/DDP combination against OS cells. We obtained 3544 targets for osteosarcoma diseases from GeneCards (Table. S1), 100 targets of CAR from Swiss Target website (Table. S2), and 8484 targets of DDP from CTD website (Table. S3). Through Venn diagram analysis, a total of 36 overlapping targets were finally obtained (Table. S4), which were probably the common molecules of CAR and DDP acting on OS (Fig. 2A). In the PPI network constructed for these targets, PTGS2 (COX2) and mTOR were identified as the most significant targets (Fig. 2B). We then focused on mTOR because this molecule is a key regulatory factor in tumor development, and inhibiting mTOR is considered promising method in tumor treatment [25, 26]. Next, we observed that the phosphorylation level of mTOR at Ser2448 which represents mTOR activation [27], was decreased by both CAR, DDP and CAR/DDP combination treatment, with the most substantial decline in CAR/DDP co-treatment group (Fig. 2C, D). Moreover, IHC results of retrieved xenograft OS samples further confirmed that reduction of mTOR phosphorylation at Ser2448 was more pronounced in CAR/DDP co-treatment group compared to the single drug group (Fig. 2E). These results indicate CAR/DDP combination may suppress the activation of mTOR in OS cells.

CAR/DDP combination promotes autophagy by inactivating mTOR

mTOR plays a crucial role in regulating autophagy. Once activated by phosphorylation, mTOR can suppress the autophagy process by blocking ULK1 complex, which includes ULK1, Atg13, Atg6, and

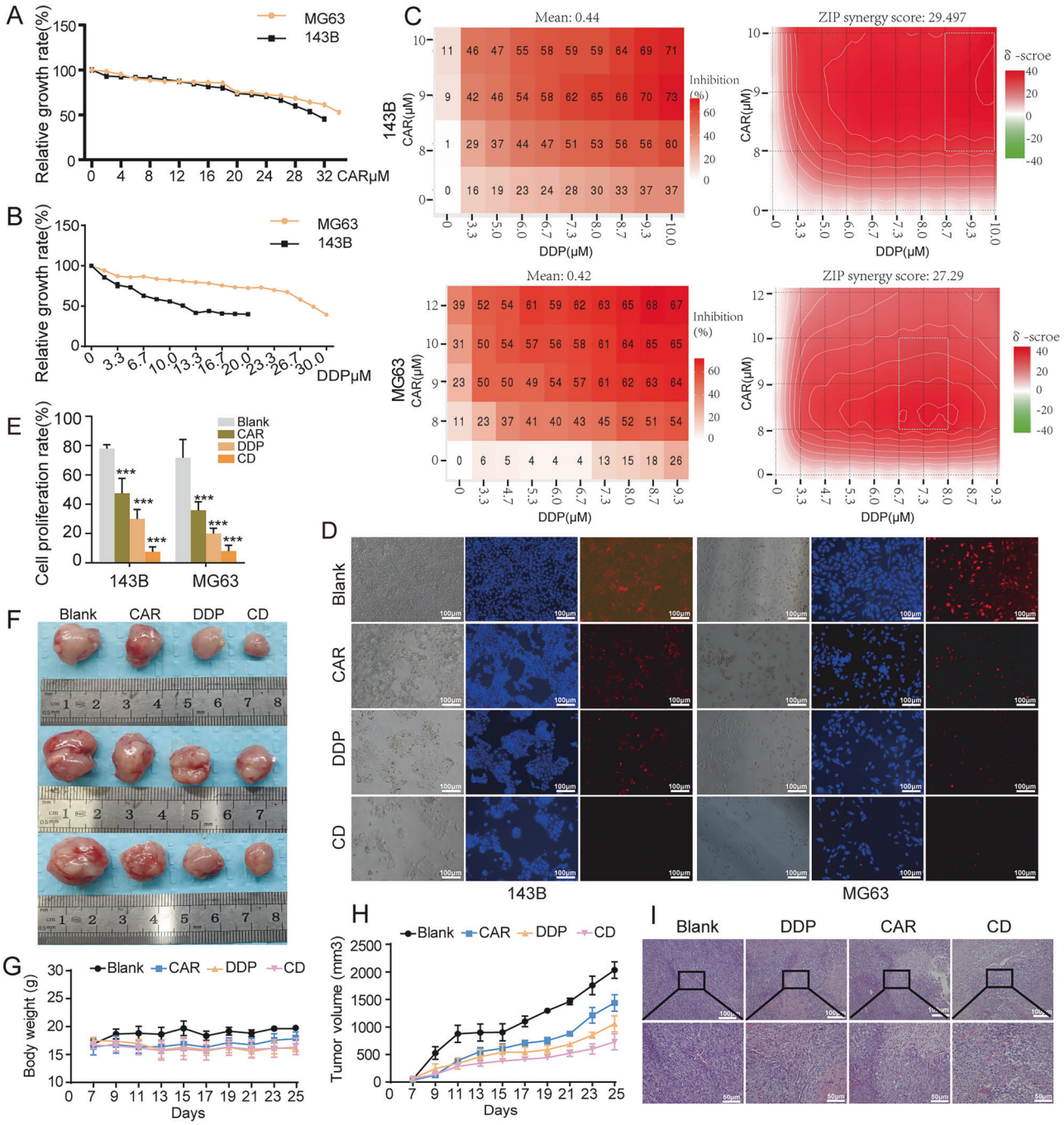

Fig. 1 CAR enhances the antitumor effect of DDP. A Cell proliferation of 143B and MG63 cells was measured by MTT assay. Cells were treated with CAR. **B** Analyzes of the effect of DDP on the proliferation of 143B and MG63 cells by MTT. **C** ZIP model analysis of CAR combined with DDP-treated 143B and MG63 cells. **D** EdU detection of proliferation rate of 143B and MG63 cells. Cells were treated with CAR, DDP, CD (CAR + DDP) respectively. **E** Quantification of the EdU results. **F** The representative mice and retrieved OS samples. **G** The weight changes of nude mice in xenograft mice model. (**H**) The volumes of retrieved OS samples. **I** H&E staining of retrieved OS sample (100×, 200×). $^{*}P < 0.05$; $^{**}P < 0.01$; $^{***}P < 0.001$.

Atg7 [28]. Since the phosphorylation of mTOR was significantly reduced by CAR/DDP combination treatment, we hypothesized that this mTOR inactivation might enhance the autophagy process. To verify our hypothesis, we infected OS cells with GFP-LC3 adenovirus, and found that GFP puncta, representing autophagosome formation, were increased in OS cells treated with CAR or DDP, while the increase was more obvious when the two were combined (Fig. 3A). To further investigate whether CAR/DDP co-treatment lead to the fusion of autophagosome with lysosome, we labeled lysosome with LysoTracker red DND-99 dye, and then evaluated the co-localization of GFP-LC3II and lysosome in 143B and MG63 cells. As expected, the co-localization of GFP-LC3II puncta with LysoTracker red DND-99 dye was markedly increased upon CAR/DPP combination treatment, implying proper autophagosome-lysosome fusion (Fig. 3B). Moreover, western blotting results (Fig. 3C, D) showed an elevated LC3II/I ratio, and increased protein levels of Beclin-1, Atg5 and Atg7 in CAR/DPP combination group. Interestingly, P62 protein levels were slightly

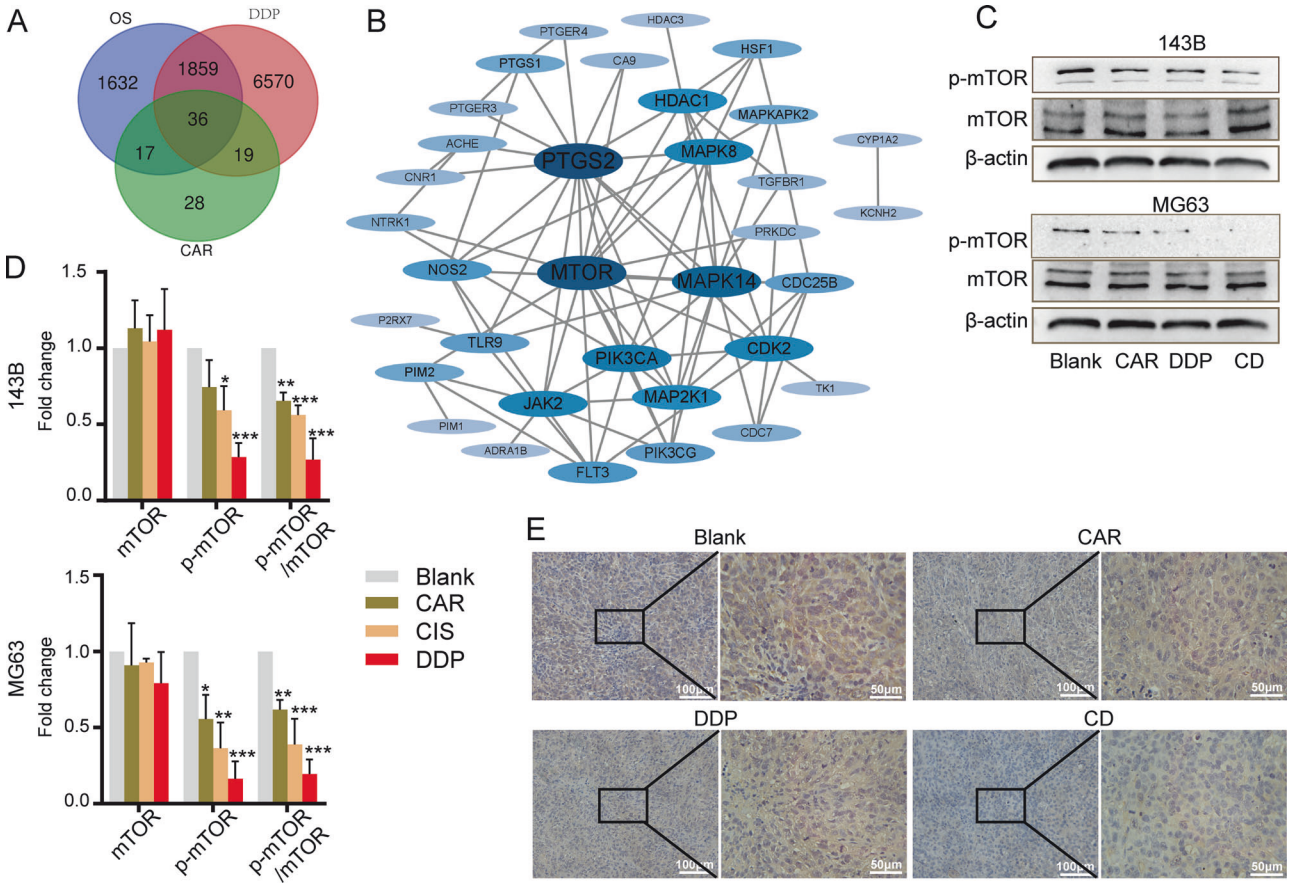

Fig. 2 The mTOR pathway is key for CAR /DDP co-treatments suppress OS cells. A OS disease targets, DDP targets and CAR targets were intersected by Venn diagram. **B** The PPI network interaction map was obtained by using Cytoscape for 36 targets. **C** Western blotting analysis of mTOR and p-mTOR expression in 143B and MG63 cells treated with previous treatment factors for 24 h. β-actin was used as a loading control. **D** Quantification of Western blotting analysis was shown. **E** IHC staining of p-mTOR protein in OS tissues (200×, 400×). $^{*}P < 0.05$; $^{**}P < 0.01$; $^{***}P < 0.001$.

increased in the single-agent groups but decreased in the combination group, while P62 mRNA levels were significantly higher in the CAR/DDP co-treatment group compared to single-agent groups (Fig. 3E). This may indicate an increase in production and degradation of P62 upon CAR/DDP co-treatment. Moreover, IHC analysis (Fig. 3F) of retrieved xenograft OS samples further confirmed that Beclin-1 upregulation was more pronounced in CAR/DDP co-treatment group than in single treatment. Next, we employed TEM to visualize ultrastructural changes of OS cells upon CAR/DDP co-treatment. The results showed that more autophagosomes were accumulated in CAR/DDP co-treated OS cells (Fig. 4A). Then we monitored autophagic flux using RFP-GFP-LC3 dual-fluorescence labeled adenovirus. As expected, there showed enhancive yellow and red puncta in CAR/DDP co-treated group (Fig. 4B), clearly indicating an increase autophagic flux in these cells. These results suggest CAR/DDP combination may promote autophagy in OS cells.

To further elucidate whether mTOR inactivation is associated with the induction of autophagy, we examined the effects of the mTOR activator (MHY) on autophagy induced by the CAR/DDP combination. TEM results (Fig. 4A) revealed that MHY treatment significantly reduced the accumulation of autophagosomes triggered by CAR/DDP combination. Additionally, MHY diminished the autophagic flux promoted by CAR/DDP combination (Fig. 4B), resulting in the less yellow and red puncta. Results of western blot further substantiated that MHY effectively attenuated the influence of CAR/DDP combination on LC3-II/I ratio, Beclin-1 protein and P62 protein levels (Fig. 4C, D). Notably, the function of autophagy inhibitor hydroxychloroquine (HCQ) on CAR/DDP combination induced autophagy were consistent with MHY (Fig. 4A, B, E, F). Together, these findings prove that CAR/DDP combination may promote autophagy by inactivating mTOR.

CAR /DDP in combination induces apoptosis of OS cells

DDP is recognized an excellent inducer of apoptosis in OS cells [29]. Our previous work has validated that CAR also triggers apoptosis in OS cells [16]. Therefore, we sought to determine whether CAR/DDP combination treatment induced more apoptosis in OS cells. Hoechst staining analysis (Fig. 5A, B) revealed that the number of nuclear pyknosis, fragmentation and dissolution in CAR/DDP co-treated OS cells was higher than that in mono-drug group, indicating the increase of apoptosis. In addition, flow cytometry analysis confirmed that CAR/DDP combination caused a noticeable apoptosis level in OS cells (Fig. 5C, D). Subsequently, western blot showed that CAR/DDP combination augmented apoptotic protein expression, including Cleaved-Caspase3, Cleaved-Parp, Cleaved-Caspase9, Bax and Bad, whereas a decrease in apoptosis inhibitory protein Bcl2 (Fig. 5E, F). Moreover, IHC results of retrieved xenograft OS samples corroborated the suppression of Bcl2 protein by the CAR/DDP combination (Fig. 5G). The above results imply that CAR/DDP combination may induce more apoptosis in OS cells.

CAR/DDP combination-induced apoptosis is probably associated with autophagy

Autophagy is believed to promote cell death (known as autophagy cell death), possibly by mediating cell apoptosis or

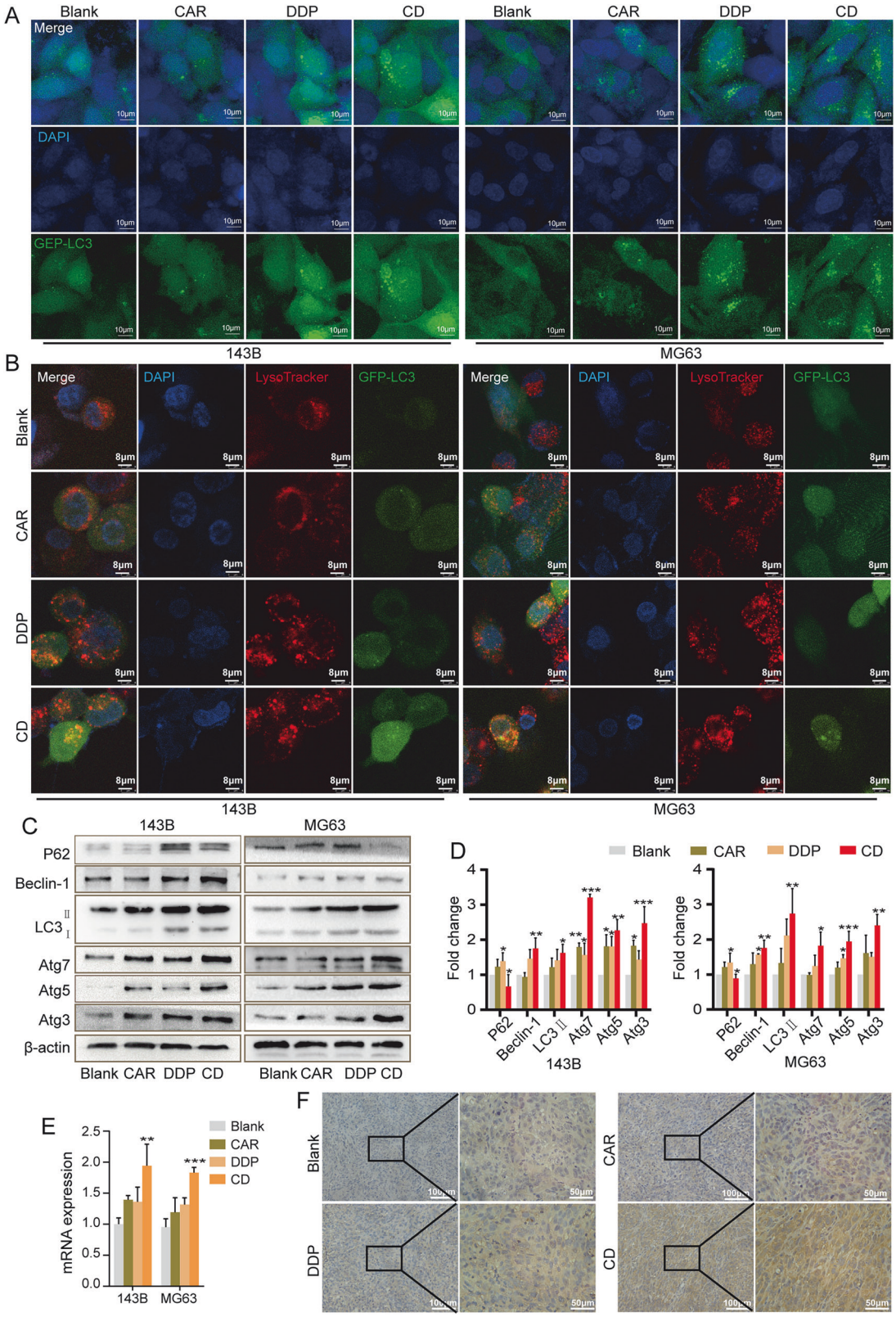

Fig. 3 CAR and DDP co-regulate autophagy in OS cells. A Confocal analysis of the LC3 puncta in 143B and MG63 cells treated with CAR, DDP, CD for 24 h respectively. **B** Effect of CAR and DDP on the colocalization of GFP-LC3 and LysoTracker in 143B and MG63 cells. Cells were treated with LysoTracker for 60 min, and images were taken under the live cell confocal microscope. The colocalization of GFP-LC3 and LysoTracker was indicated by the number of yellow spots in the merged images. **C** Western blotting analysis of P62, Beclin-1, LC3I/II, Atg7, Atg5 and Atg3 expression in 143B and MG63 cells treated with previous treatment factors for 24 h. β-actin was used as a loading control. **D** Quantification of Western blotting analysis were shown. **E** The mRNA level expression of P62 in 143B and MG63 cells treated with CAR, DDP and CD for 24 h respectively. **F** IHC staining of Beclin-1 levels in OS tissues (200×, 400×). $^{*}P < 0.05$; $^{**}P < 0.01$; $^{***}P < 0.001$.

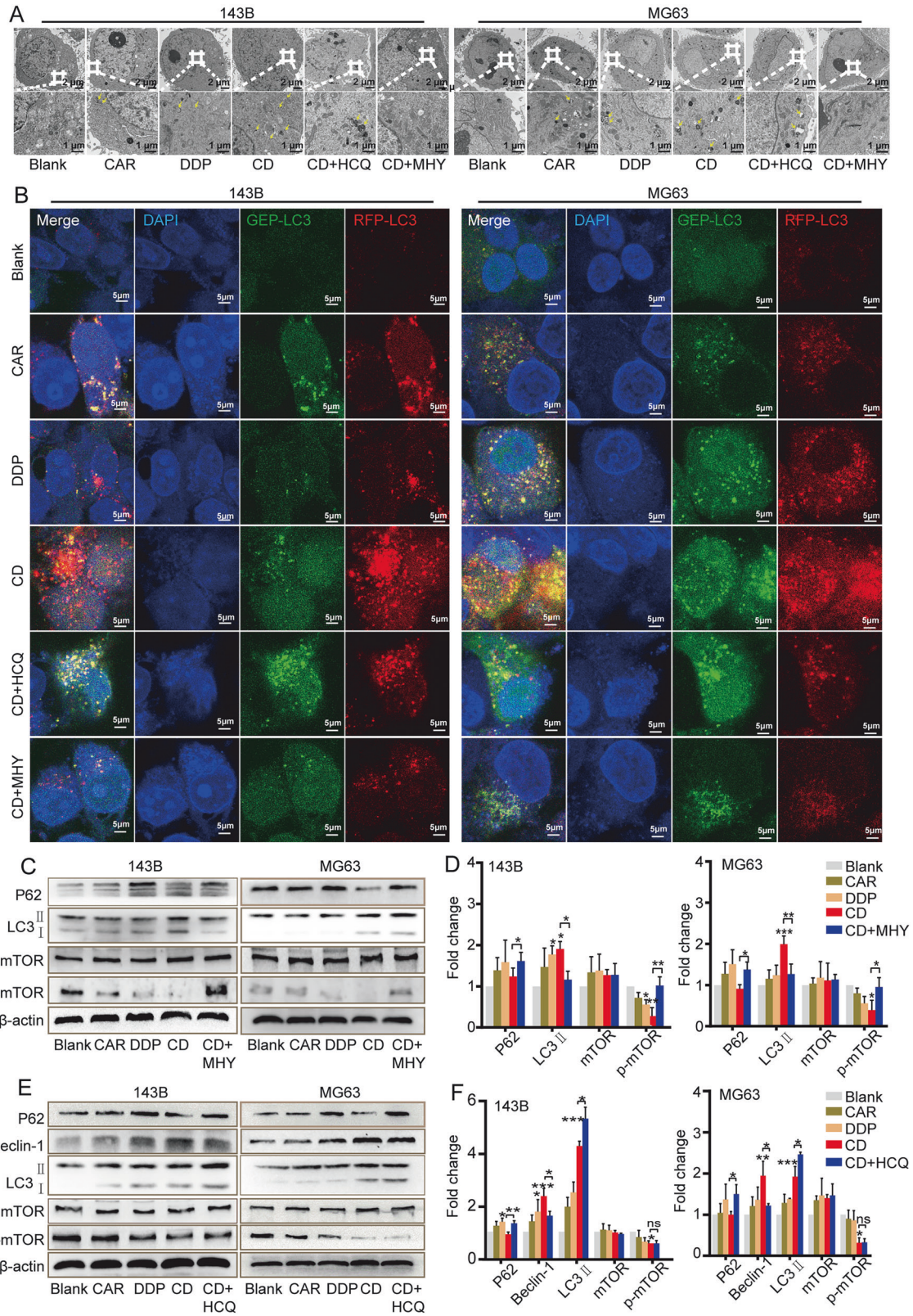

Fig. 4 CAR/DDP combination promotes autophagy by reducing mTOR in OS cells. A 143B and MG63 cells were treated with CAR/DDP in the presence or absence of HCQ (10 μM) and MHY (100 nM). TEM images were selected. Scale bars are 2 and 1 μM for photographs in boxed areas. **B** 143B and MG63 cells were transfected with RFP-GFP-LC3 dual-fluorescence adenovirus, after co-incubation with CAR/DDP in the presence or absence of HCQ (10 μM) and MHY (100 nM). Confocal analysis of the LC3 puncta. **C** Western blotting analysis of P62, LC3II/I, p-mTOR and mTOR expression in 143B and MG63 cells treated with CAR/DDP in the presence or absence of MHY (100 nM) for 24 h. β-actin was used as a loading control. **D** Quantification of Western blotting analysis was shown. **E** Western blotting analysis of P62, Beclin-1, LC3II/I, p-mTOR and mTOR expression in 143B and MG63 cells treated with CAR/DDP in the presence or absence of HCQ (10 μM) for 24 h. β-actin was used as a loading control. **F** Quantification of Western blotting analysis was shown. $^{*}P < 0.05$; $^{**}P < 0.01$; $^{***}P < 0.001$.

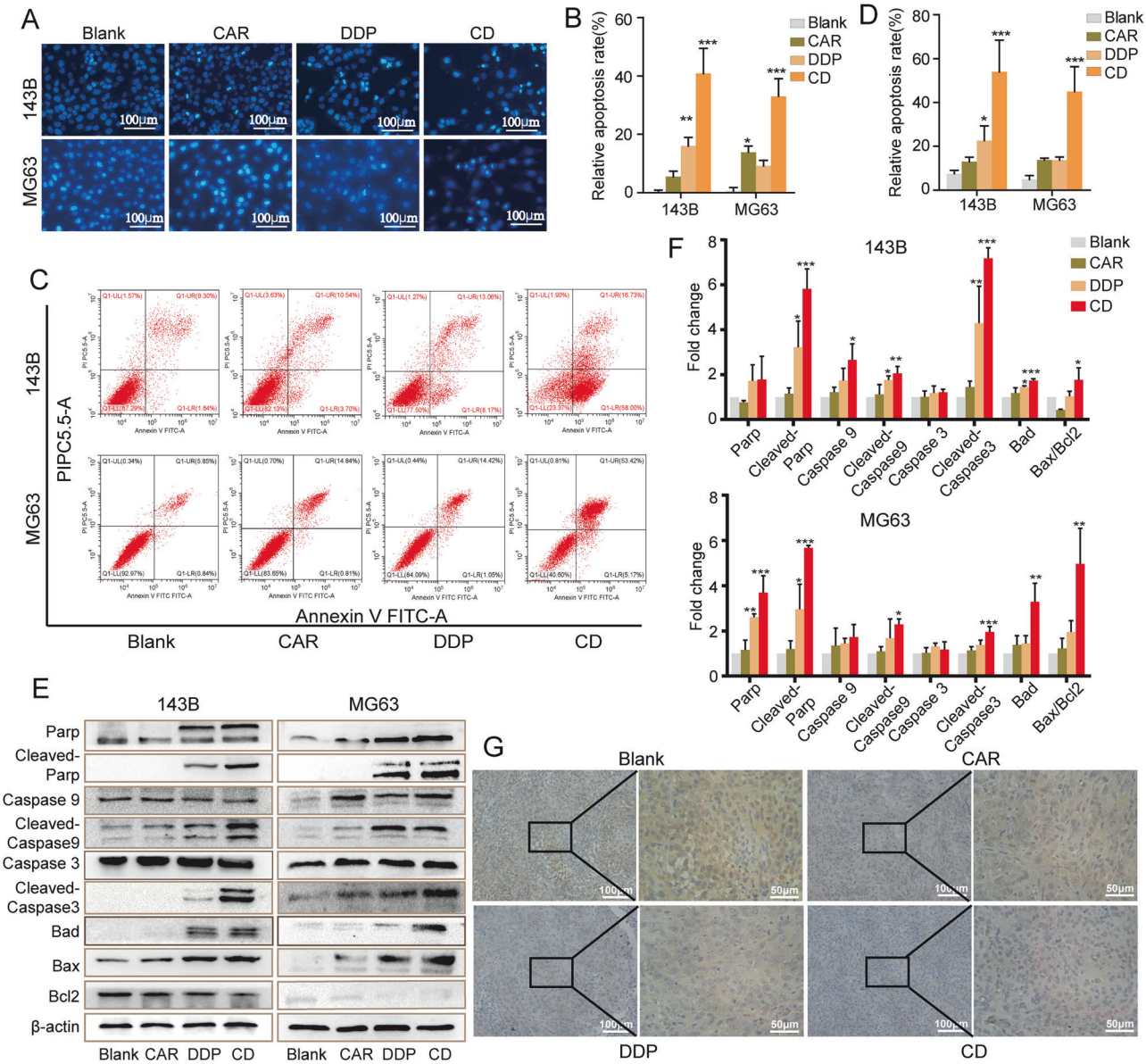

Fig. 5 CAR/DDP in combination induces apoptosis in OS cells. **A** Cell apoptosis of 143B and MG63 cells was measured by Hoechst33258 staining. Cells were treated with CAR, DDP, CD respectively. **B** Quantitative results of (**A**). **C** Cell apoptosis of 143B and MG63 cells was measured by flow cytometry analysis of Annexin-V/PI double staining. **D** Quantification of apoptosis. **E** Western blotting analysis of Parp, Cleaved-Parp, Caspase9, Cleaved-Caspase9, Caspase3, Cleaved-Caspase3, Bad, Bax as well as Bcl2 expression in 143B and MG63 cells treated with previous treatment factors for 24 h. β-actin was used as a loading control. **F** Quantification of Western blotting analysis was shown. **G** IHC staining of Bcl2 levels in OS tissues (200×, 400×). $*P < 0.05$; $**P < 0.01$; $***P < 0.001$.

necrosis through excessive autophagy flux [30]. Our above results have suggested that CAR/DDP co-treatment can promote autophagy and apoptosis in OS cells.

To explore the link between these two processes, we utilized Hoechst33258 staining and discovered that autophagy inhibitor HCQ and mTOR activator MHY both suppressed the apoptosis induced by CAR/DDP co-administration in OS cells (Fig. 6A, B). Furthermore, HCQ and MHY partially restored the viability of OS cells under CAR/DDP co-treatment (Fig. 6C), suggesting that they can mitigate the apoptosis induced by the CAR/DDP combination. Additionally, we found that both MHY and HCQ reversed the increased level of Cleaved-Caspase3 and the decreased level of Bcl2 induced by CAR/DDP combination (Fig. 6D–G). Hence, these results validated that CAR/DDP combination-induced apoptosis is probably associated with autophagy.

CAR attenuates DDP resistance by enhancing autophagy

Subsequently, we used crystal violet staining experiment (Fig. 7A, B) and MTT experiment (Fig. 7C) to screen for DDP concentrations with the same inhibition rate as CD group in OS cells. We found that achieving same effect requires 14.0 μM DDP. Further analysis using GFP-LC3 detection (Fig. 7D) revealed that although cells growth rate in DDP was consistent with CD group, the level of autophagy was higher in combined treatment. Given that studies have implicated autophagy in DDP resistance in cancer therapy [31], we then conducted experiments to examine the effects in OS DDP-resistant cell lines (HOS/DDP) (Fig. 7E, F). We observed that cell growth rate was lower when treated with CD co-treatment, suggesting CAR can reduce DDP resistance to some extent. However, the addition of HCQ partially inhibit the effect of CD, indicating that reduction of DDP resistance by CAR may be associated with the enhancement of autophagy.

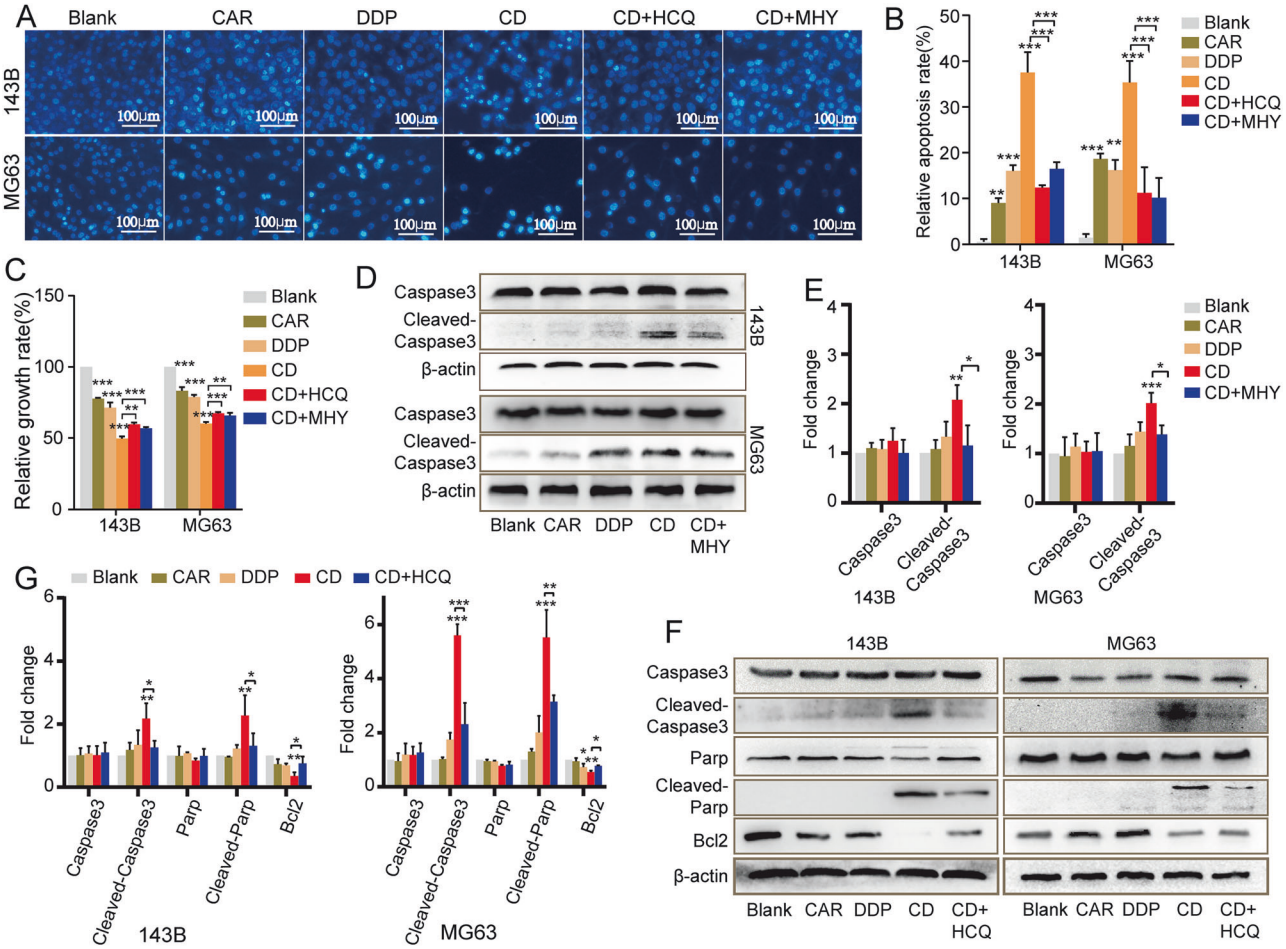

Fig. 6 CAR/DDP in combination induces apoptosis in OS cells through autophagy. A Cell apoptosis of 143B and MG63 cells was measured by Hoechst33258 staining. Cells were treated with CAR, DDP, CD in the presence or absence of HCQ (10 μM) and MHY (100 nM). **B** Quantitative results of (**A**). **C** Cell apoptosis of 143B and MG63 cells was measured by MTT assay. **D** Western blotting analysis of Caspase3 and Cleaved-Caspase3 expression in 143B and MG63 cells treated with CAR/DDP in the presence or absence of MHY (100 nM). β-actin was used as a loading control. **E** Quantification of Western blotting analysis was shown. **F** Western blotting analysis of Caspase3, Cleaved-Caspase3, Parp, Cleaved-Parp and Bcl2 expression in 143B and MG63 cells treated with CAR/DDP in the presence or absence of HCQ (10 μM). β-actin was used as a loading control. **G** Quantification of Western blotting analysis was shown. $^{*}P < 0.05$; $^{**}P < 0.01$; $^{***}P < 0.001$.

DISCUSSION

DDP, commonly used chemotherapy drug, exerts its anti-cancer activity through diverse mechanisms. In addition to inhibiting DNA replication [32], it can also cause necrosis or apoptosis by activating multiple transduction pathways, including Rad9-Hus1-Rad1-ATR-Chk1 pathway, DNA-Pt-HMGB1 ternary complex and p53 pathway, etc [33, 34]. Unfortunately, in some cases, DDP did not demonstrate optimal efficacy due to adverse effects and drug resistance. The suboptimal DDP treatment effect can be attributed to multifarious factors, including decreased drug accumulation, drug inactivation through binding with different proteins, the enhancement of DNA repair, and the alterations of drug-resistant related proteins [35]. Fortunately, the disadvantages of DDP can be overcome by combining with other drugs. This approach has the potential to reduce side effects, produce optimized synergic anti-OS effects and improve treatment efficacy [36].

NPs are defined as chemicals derived from plants, microbes and other marine organisms. Recent research indicates that since 2000, more than 120 distinct NPs databases and collections have been released [37]. In contrast to traditional chemotherapy, NPs are relatively inexpensive and have low risk of side effects. Moreover, they are frequently combined with DDP to enhance its anti-tumor efficacy [38]. For instance, Anemoside B4 has been shown to mitigate DDP-induced nephrotoxicity without compromising its antitumor efficacy [39]. Berberine in combination with DDP induces necrotizing apoptosis in ovarian cancer cells [40]. Our previous research has also demonstrated that CAR effectively inhibits OS cells growth with minimal toxic side effects against human normal cells [16]. Motivated by these findings, we explored the potential synergistic effect of CAR with DDP on OS cells. The results demonstrated that combination of CAR and DDP exhibited a synergistic effect on the proliferation of 143B and MG63 OS cells in vitro, as well as on the xenograft OS growth of 143B cells in vivo. Notably, the CAR/DDP combination led to a significant reduction in mTOR phosphorylation compared to monotherapy, suggesting mTOR inactivation. mTOR, a central regulator of cellular metabolism, is often hyperactivated in cancer, driving tumor cell growth and metabolism [25, 26]. Furthermore, mTOR is also pivotal regulatory molecule of autophagy. Conditions conducive to autophagy induction such as nutrient or growth factor deprivation and low cellular energy levels have been shown to inhibit mTOR activity [41], suggesting tight inverse coupling between autophagy induction and mTOR activation.

Autophagy is the collective term for all pathways that transport cytoplasmic substances to lysosomes in animal cells or vacuoles in plant and yeast cells [42]. Based on packaging materials and delivery mechanisms, autophagy is divided into three main types: macroautophagy, microautophagy, and chaperone-mediated

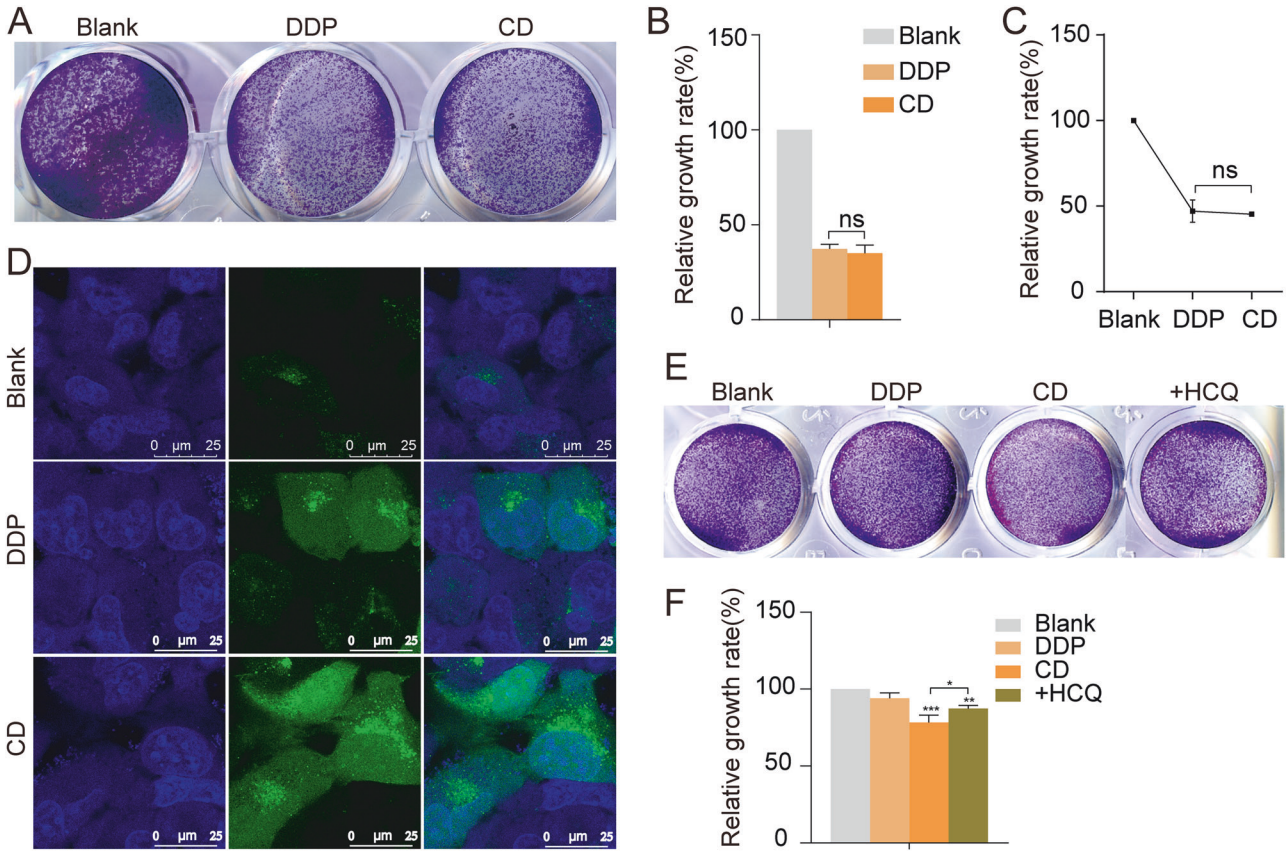

Fig. 7 CAR reduces DDP resistance. A Cell viability of HOS cells was measured by crystal violet staining assay. Cells were treated with DDP and CD respectively. **B** Quantification of the crystal violet staining. **C** Cell viability of HOS cells was measured by MTT assay. **D** Confocal analysis of the LC3 puncta in HOS cells treated with DDP and CD for 24 h. **E** Crystal violet assay for detecting cell growth rate. **F** Quantification of the crystal violet staining. *$P < 0.05$; **$P < 0.01$; ***$P < 0.001$.

autophagy [42]. During the occurrence of autophagy, there are a variety of autophagy-related proteins that precisely regulate various critical nodes of autophagy [43]. Among these molecules, Beclin-1 is particularly important, as it mediates the localization of autophagy-related proteins in phagocytic vesicles and regulates formation and maturation of autophagosomes [44]. LC3I is converted to LC3II through Atg3 and Atg7-mediated ubiquitination, which also plays a role in autophagy [45, 46]. In our study, we observed that combination of CAR and DDP promoted accumulation of LC3II and Beclin-1 in OS cells, suggesting an upregulation of autophagy following the combined treatment. It is noteworthy that following CAR/DDP combined treatment, there was an increase in mRNA levels of P62 while P62 protein levels decreased. We speculated that this might be a feedback mechanism of OS cells to CAR/DPP co-treatment-induced P62 degradation. The recognition of ubiquitinated protein aggregates and their delivery to autophagosomes requires proteins containing an ubiquitin-binding domain, P62 is the most intensively studied one of these aptamers [47]. It is capable of recognizing and binding ubiquitinated proteins through its UBA domain, subsequently interacting with the core autophagic protein LC3 through the LIR domain [48, 49]. During autophagic lysosomal degradation, P62, which accelerates the recruitment and isolation of ubiquitinated proteins, is degraded by Ubiquitination-proteasomes [50]. Thus, the increase in P62 consumption is often indicative of heightened autophagy activity. In this study, after adding MHY, the p-mTOR protein level that was reduced during combined CAR/DPP treatment was restored and the increased autophagy levels were reduced accordingly. This suggests that CAR/DDP may enhance autophagy by reducing p-mTOR levels.

Autophagy is essential for cellular homeostasis, as it eliminates dysfunctional organelles, protein clumps, and damaged large molecules, also recycling breakdown products [51]. Eukaryotic cells have basal levels of autophagy, which is responsible for monitoring cytoplasmic components and ensuring cellular homeostasis. This process can be rapidly unregulated under various pathological conditions (e.g. starvation, oxidative stress, etc.) [52]. However, the debate continues whether autophagy inhibits cancer cells or promotes their survival during chemotherapy-induced stress. While some studies suggest that autophagy contributes to cancer cells' resistance to chemotherapy. Therefore, blocking autophagy could potentially improve the effectiveness of anticancer treatments by making cancer cells more responsive to chemotherapy [53]. However, others propose that autophagy could serve as a process for cancer cell demise by potentially amplifying the impact of chemotherapy and radiotherapy in triggering cell death [31, 54]. In this study, we observed that CAR/DDP combination enhanced the autophagy level in OS cells, and reduced DDP resistance through autophagy.

This study also validated that the CAR/DDP combination-induced apoptosis may be highly correlated with autophagy. Research has indicated that Bcl2 and Beclin-1 may be the link between autophagy and apoptosis [47, 55]. Anti-apoptotic Bcl2, a key member of the Bcl family, is essential for regulating programmed cell death through controlling intracellular apoptotic signals [56]. Beclin-1, essential for the formation of autophagic structures, can interact with Bcl2, potentially impairing autophagosome formation and leading to maturation disorders [57]. Certain research indicates that caspases, which play a role in triggering autophagy through apoptosis, are primarily involved in

degradation Bcl2-associated transcription factor 1 (BCLAF1) [58, 59]. However, in certain instances, this degradation can become constitutively activated, which turns competitive disruption of the Bcl2-Beclin-1 complex into an increase in interaction of BCLAF1 with Bcl2, ultimately leading to an increase in autophagic flow-mediated cell death [60]. Our study showed that CAR/DDP co-treatment elevated Beclin-1 protein level while concomitantly reducing Bcl2 protein level. We therefore hypothesized that the impact of CAR/DDP co-treatment on autophagy and apoptosis may be partly caused by the Bcl2 and Beclin-1 interaction. However, more evidence is required to validate this hypothesis.

CONCLUSIONS

Our findings confirm that CAR can significantly enhance the inhibitory effects of DDP on OS cell growth in vitro and in vivo. Moreover, CAR/DDP combination appears to induce autophagy in OS cells through inactivating mTOR, and CAR attenuates DDP resistance through autophagy. The mTOR-mediated induction of autophagy by CAR/DDP combination may be essential for their synergistic anti-OS effects, because autophagy inhibitor HCQ and mTOR activator MHY can not only impair autophagy but also attenuate apoptosis and restore viability in CAR/DDP co-treated OS cells.

DATA AVAILABILITY

Data will be made available on request.

REFERENCES

1. Beird HC, Bielack SS, Flanagan AM, Gill J, Heymann D, Janeway KA. et al. Osteosarcoma. Nat Rev Dis Prim. 2022;8:77
2. Yan GN, Lv YF, Guo QN. Advances in osteosarcoma stem cell research and opportunities for novel therapeutic targets. Cancer Lett. 2016;370:268–74.
3. Cortini M, Avnet S, Baldini N. Mesenchymal stroma: role in osteosarcoma progression. Cancer Lett. 2017;405:90–9.
4. Isakoff MS, Bielack SS, Meltzer P, Gorlick R. Osteosarcoma: current treatment and a collaborative pathway to success. J Clin Oncol. 2015;33:3029–35.
5. Lagmay JP, Krailo MD, Dang H, Kim A, Hawkins DS, Beaty O, 3rd. et al. Outcome of patients with recurrent osteosarcoma enrolled in seven phase II trials through Children's Cancer Group, pediatric oncology group, and children's oncology group: learning from the past to move forward. J Clin Oncol. 2016;34:3031–8.
6. Whelan JS, Davis LE. Osteosarcoma, chondrosarcoma, and chordoma. J Clin Oncol. 2018;36:188–93.
7. Meyers PA, Schwartz CL, Krailo MD, Healey JH, Bernstein ML, Betcher D. et al. Osteosarcoma: the addition of muramyl tripeptide to chemotherapy improves overall survival-a report from the Children's Oncology Group. J Clin Oncol : J Am Soc Clin Oncol. 2008;26:633–8.
8. Marina NM, Smeland S, Bielack SS, Bernstein M, Jovic G, Krailo MD. et al. Comparison of MAPIE versus MAP in patients with a poor response to preoperative chemotherapy for newly diagnosed high-grade osteosarcoma (EURAMOS-1): an open-label, international, randomised controlled trial. Lancet Oncol. 2016;17:1396–408.
9. Gaspar N, Occean BV, Pacquement H, Bompas E, Bouvier C, Brisse HJ. et al. Results of methotrexate-etoposide-ifosfamide based regimen (M-EI) in osteosarcoma patients included in the French OS2006/sarcome-09 study. Eur J cancer (Oxf, Engl : 1990). 2018;88:57–66.
10. Huang H, Lu Q, Yuan X, Zhang P, Ye C, Wei M. et al. Andrographolide inhibits the growth of human osteosarcoma cells by suppressing Wnt/β-catenin, PI3K/AKT and NF-κB signaling pathways. Chem-Biol Interact. 2022;365:110068
11. Alizadehnohi M, Nabiuni M, Nazari Z, Safaeinejad Z, Irian S. The synergistic cytotoxic effect of cisplatin and honey bee venom on human ovarian cancer cell line A2780cp. J Venom Res. 2012;3:22–7.
12. Lu Q, Huang H, Wang X, Luo L, Xia H, Zhang L. et al. Echinatin inhibits the growth and metastasis of human osteosarcoma cells through Wnt/β-catenin and p38 signaling pathways. Pharmacol Res. 2023;191:106760
13. Ruibin J, Bo J, Danying W, Jianguo F, Linhui G. Cardamonin induces G2/M phase arrest and apoptosis through inhibition of NF-κB and mTOR pathways in ovarian cancer. Aging. 2020;12:25730–43.
14. Liao NC, Shih YL, Ho MT, Lu TJ, Lee CH, Peng SF. et al. Cardamonin induces immune responses and enhances survival rate in WEHI-3 cell-generated mouse leukemia in vivo. Environ Toxicol. 2020;35:457–67.
15. Cardenas Garza GR, Elizondo Luevano JH, Bazaldua Rodriguez AF, Chavez Montes A, Perez Hernandez RA, Martinez Delgado AJ, et al. Benefits of cardamom (Elettaria cardamomum (L.) Maton) and turmeric (Curcuma longa L.) extracts for their applications as natural anti-inflammatory adjuvants. Plants. 2021;10:1908–25.
16. Zhang L, Yang C, Huang Y, Huang H, Yuan X, Zhang P. et al. Cardamonin inhibits the growth of human osteosarcoma cells through activating P38 and JNK signaling pathway. Biomed Pharmacother Biomed Pharmacother. 2021;134:111155
17. Ianevski A, Lahtela J, Javarappa KK, Sergeev P, Ghimire BR, Gautam P, et al. Patient-tailored design for selective co-inhibition of leukemic cell subpopulations. Sci Adv. 2021;7:1126.
18. Kim S, Thiessen PA, Bolton EE, Chen J, Fu G, Gindulyte A. et al. PubChem substance and compound databases. Nucleic Acids Res. 2016;44:D1202–13.
19. Gfeller D, Michielin O, Zoete V. Shaping the interaction landscape of bioactive molecules. Bioinformatics. 2013;29:3073–9.
20. Wang X, Shen Y, Wang S, Li S, Zhang W, Liu X. et al. PharmMapper 2017 update: a web server for potential drug target identification with a comprehensive target pharmacophore database. Nucleic Acids Res. 2017;45:W356–w60.
21. Davis AP, Murphy CG, Saraceni-Richards CA, Rosenstein MC, Wiegers TC, Mattingly CJ. Comparative Toxicogenomics Database: a knowledgebase and discovery tool for chemical-gene-disease networks. Nucleic Acids Res. 2009;37:D786–92.
22. Pichler K, Warner K, Magrane M. SPIN: submitting sequences determined at protein level to UniProt. Curr Protoc Bioinform. 2018;62:e52
23. Safran M, Solomon I, Shmueli O, Lapidot M, Shen-Orr S, Adato A. et al. GeneCards 2002: towards a complete, object-oriented, human gene compendium. Bioinformatics. 2002;18:1542–3.
24. Szklarczyk D, Gable AL, Lyon D, Junge A, Wyder S, Huerta-Cepas J. et al. STRING v11: protein-protein association networks with increased coverage, supporting functional discovery in genome-wide experimental datasets. Nucleic Acids Res. 2019;47:D607–13.
25. Laplante M, Sabatini DM. mTOR signaling in growth control and disease. Cell. 2012;149:274–93.
26. Mossmann D, Park S, Hall MN. mTOR signalling and cellular metabolism are mutual determinants in cancer. Nat Rev Cancer. 2018;18:744–57.
27. Lawrence JC, Lin TA, McMahon LP, Choi KM. Modulation of the protein kinase activity of mTOR. Curr Top Microbiol Immunol. 2004;279:199–213.
28. Kim J, Kundu M, Viollet B, Guan KL. AMPK and mTOR regulate autophagy through direct phosphorylation of Ulk1. Nat Cell Biol. 2011;13:132–41.
29. Zhu J, Zou H, Yu W, Huang Y, Liu B, Li T. et al. Checkpoint kinase inhibitor AZD7762 enhance cisplatin-induced apoptosis in osteosarcoma cells. Cancer Cell Int. 2019;19:195
30. Baehrecke EH. Autophagy: Dual roles in life and death?. Nat Rev Mol Cell Biol. 2005;6:505–10.
31. Wright TJ, McKee C, Birch-Machin MA, Ellis R, Armstrong JL, Lovat PE. Increasing the therapeutic efficacy of docetaxel for cutaneous squamous cell carcinoma through the combined inhibition of phosphatidylinositol 3-kinase/AKT signalling and autophagy. Clin Exp Dermatol. 2013;38:421–3.
32. Florea AM, Busselberg D. Cisplatin as an anti-tumor drug: cellular mechanisms of activity, drug resistance and induced side effects. Cancers. 2011;3:1351–71.
33. Wagner JM, Karnitz LM. Cisplatin-induced DNA damage activates replication checkpoint signaling components that differentially affect tumor cell survival. Mol Pharm. 2009;76:208–14.
34. Jamieson ER, Lippard SJ. Structure, recognition, and processing of cisplatin-DNA adducts. Chem Rev. 1999;99:2467–98.
35. Skowron MA, Melnikova M, van Roermund JGH, Romano A, Albers P, Thomale J, et al. Multifaceted mechanisms of cisplatin resistance in long-term treated urothelial carcinoma cell lines. Int J Mol Sci. 2018;19:590–607.
36. Pasello M, Michelacci F, Scionti I, Hattinger CM, Zuntini M, Caccuri AM. et al. Overcoming glutathione S-transferase P1-related cisplatin resistance in osteosarcoma. Cancer Res. 2008;68:6661–8.
37. Sorokina M, Steinbeck C. Review on natural products databases: where to find data in 2020. J Cheminform. 2020;12:20
38. Ridzuan NRA, Rashid NA, Othman F, Budin SB, Hussan F, Teoh SL. Protective role of natural products in cisplatin-induced nephrotoxicity. Mini Rev Med Chem. 2019;19:1134–43.
39. He L, Zhang Y, Kang N, Wang Y, Zhang Z, Zha Z. et al. Anemoside B4 attenuates nephrotoxicity of cisplatin without reducing anti-tumor activity of cisplatin. Phytomed Int J Phytother Phytopharmacol. 2019;56:136–46.
40. Liu L, Fan J, Ai G, Liu J, Luo N, Li C. et al. Berberine in combination with cisplatin induces necroptosis and apoptosis in ovarian cancer cells. Biol Res. 2019;52:37

41. Xiong Y, Yepuri G, Forbiteh M, Yu Y, Montani JP, Yang Z. et al. ARG2 impairs endothelial autophagy through regulation of MTOR and PRKAA/AMPK signaling in advanced atherosclerosis. Autophagy. 2014;10:2223–38.
42. Mizushima N, Komatsu M. Autophagy: renovation of cells and tissues. Cell. 2011;147:728–41.
43. Wollert T. Autophagy. Curr Biol CB. 2019;29:R671–7.
44. Matsunaga K, Saitoh T, Tabata K, Omori H, Satoh T, Kurotori N. et al. Two Beclin 1-binding proteins, Atg14L and Rubicon, reciprocally regulate autophagy at different stages. Nat Cell Biol. 2009;11:385–96.
45. Suzuki K, Kubota Y, Sekito T, Ohsumi Y. Hierarchy of Atg proteins in pre-autophagosomal structure organization. Genes Cells Devoted Mol Cell Mech. 2007;12:209–18.
46. Ichimura Y, Kirisako T, Takao T, Satomi Y, Shimonishi Y, Ishihara N. et al. A ubiquitin-like system mediates protein lipidation. Nature. 2000;408:488–92.
47. Lamark T, Svenning S, Johansen T. Regulation of selective autophagy: the p62/SQSTM1 paradigm. Essays Biochem. 2017;61:609–24.
48. Zhang W, Meng Y, Liu N, Wen XF, Yang T. Insights into chemoresistance of prostate cancer. Int J Biol Sci. 2015;11:1160–70.
49. Rah B, ur Rasool R, Nayak D, Yousuf SK, Mukherjee D, Kumar LD, et al. PAWR-mediated suppression of BCL2 promotes switching of 3-azido withaferin A (3-AWA)-induced autophagy to apoptosis in prostate cancer cells. Autophagy. 2015;11:314–31.
50. Raasi S, Varadan R, Fushman D, Pickart CM. Diverse polyubiquitin interaction properties of ubiquitin-associated domains. Nat Struct Mol Biol. 2005;12:708–14.
51. Galluzzi L, Pietrocola F, Levine B, Kroemer G. Metabolic control of autophagy. Cell. 2014;159:1263–76.
52. Kroemer G, Mariio G, Levine B. Autophagy and the integrated stress response. Mol Cell. 2010;40:280–93.
53. Su YC, Davuluri GV, Chen CH, Shiau DC, Chen CC, Chen CL. et al. Galectin-1-induced autophagy facilitates cisplatin resistance of hepatocellular carcinoma. PloS ONE. 2016;11:e0148408
54. Rosenfeld MR, Ye X, Supko JG, Desideri S, Grossman SA, Brem S. et al. A phase I/II trial of hydroxychloroquine in conjunction with radiation therapy and concurrent and adjuvant temozolomide in patients with newly diagnosed glioblastoma multiforme. Autophagy. 2014;10:1359–68.
55. Ehrlicher SE, Stierwalt HD, Miller BF, Newsom SA, Robinson MM. Mitochondrial adaptations to exercise do not require Bcl2-mediated autophagy but occur with BNIP3/Parkin activation. FASEB J. 2020;34:4602–18.
56. Siddiqui WA, Ahad A, Ahsan H. The mystery of BCL2 family: Bcl-2 proteins and apoptosis: an update. Arch Toxicol. 2015;89:289–317.
57. Castro-Gonzalez S, Shi Y, Colomer-Lluch M, Song Y, Mowery K, Almodovar S. et al. HIV-1 Nef counteracts autophagy restriction by enhancing the association between BECN1 and its inhibitor BCL2 in a PRKN-dependent manner. Autophagy. 2021;17:553–77.
58. Tsapras P, Nezis IP. Caspase involvement in autophagy. Cell Death Differ. 2017;24:1369–79.
59. Fan TJ, Han LH, Cong RS, Liang J. Caspase family proteases and apoptosis. Acta Biochim Biophys Sin. 2005;37:719–27.
60. Lamy L, Ngo VN, Emre NC, Shaffer AL, 3rd, Yang Y, Tian E. et al. Control of autophagic cell death by caspase-10 in multiple myeloma. Cancer Cell. 2013;23:435–49.

ACKNOWLEDGEMENTS

We are grateful for the expert advice of Dr. Jinyong Luo (Chongqing Medical University, Chongqing, China).

AUTHOR CONTRIBUTIONS

Sheng Li: Conceptualization, Methodology, Validation, Project administration; Ziyun Li: Project administration, Investigation; Jiayu Wang: Supervision; Xueqian Han: Resources, Software; Lulu Zhang: Methodology, Validation, Formal analysis, Writing - Original Draft.

FUNDING

Consent to participate by the Natural Science Foundation Project of Chongqing Science and Technology Commission (Grant numbers: CSTB2022TIAD-YJX0001).

COMPETING INTERESTS

The authors declare no competing interests.

ETHICAL APPROVAL

This study was conducted in accordance with relevant guidelines and regulations. The research involving animal experiments was approved by the laboratory animal research ethics committee at Chongqing Medical University (Approval No. 2022164). All animal care and experimental procedures adhered to the guidelines outlined in the *Guide for the Care and Use of Laboratory Animals*. No identifiable images or other personal data of participants were used in this study.

ADDITIONAL INFORMATION

Supplementary information The online version contains supplementary material available at https://doi.org/10.1038/s41417-025-00894-9.

Correspondence and requests for materials should be addressed to Lulu Zhang.

Reprints and permission information is available at http://www.nature.com/reprints

Publisher's note Springer Nature remains neutral with regard to jurisdictional claims in published maps and institutional affiliations.